SUPPLEMENTARY INFORMATION

1 Probability densities : dependence on the central particle radius

The model presented in the article allows for the calculation of the conditional probability density of neighbours, $P(n|r_c)$, contacts, $P(z|r_c)$, and local packing fraction, $P(\phi_{loc}|r_c)$, for a given central particle radius r_c. We integrate these densities against the radius distribution $P(r)$ to obtain the overall distributions, for example

$$P(z) = \int dr\ P(z,r) = \int dr\ P(r)P(z|r).$$

The results presented in Fig. 3 of the article show that the averaged distributions computed using the model agree with the experiment. A more detailed test of this agreement is to compare the conditional probabilities with experimental results, to see if the model captures the dependence on the central particle radius. These comparisons are presented in Figs. A, B and C. Experimental data is plotted as circles, whose area is proportional to the number of observations. These circles are overplotted on a colour map of probability obtained from the model. It can be seen that the model quantitatively captures the dependence of r_c for the local packing fraction (Fig. A), the number of neighbours (Fig. B) and the number of contacts (Fig. C). In addition, we show the probability distributions for each given radius r_c in the gallery of graphs in Figs. (D, E and F) for a more detailed comparison. Due to the broad radius distribution of the emulsion droplets, some of the histograms lack statistics, nevertheless, the trends are successfully reproduced.

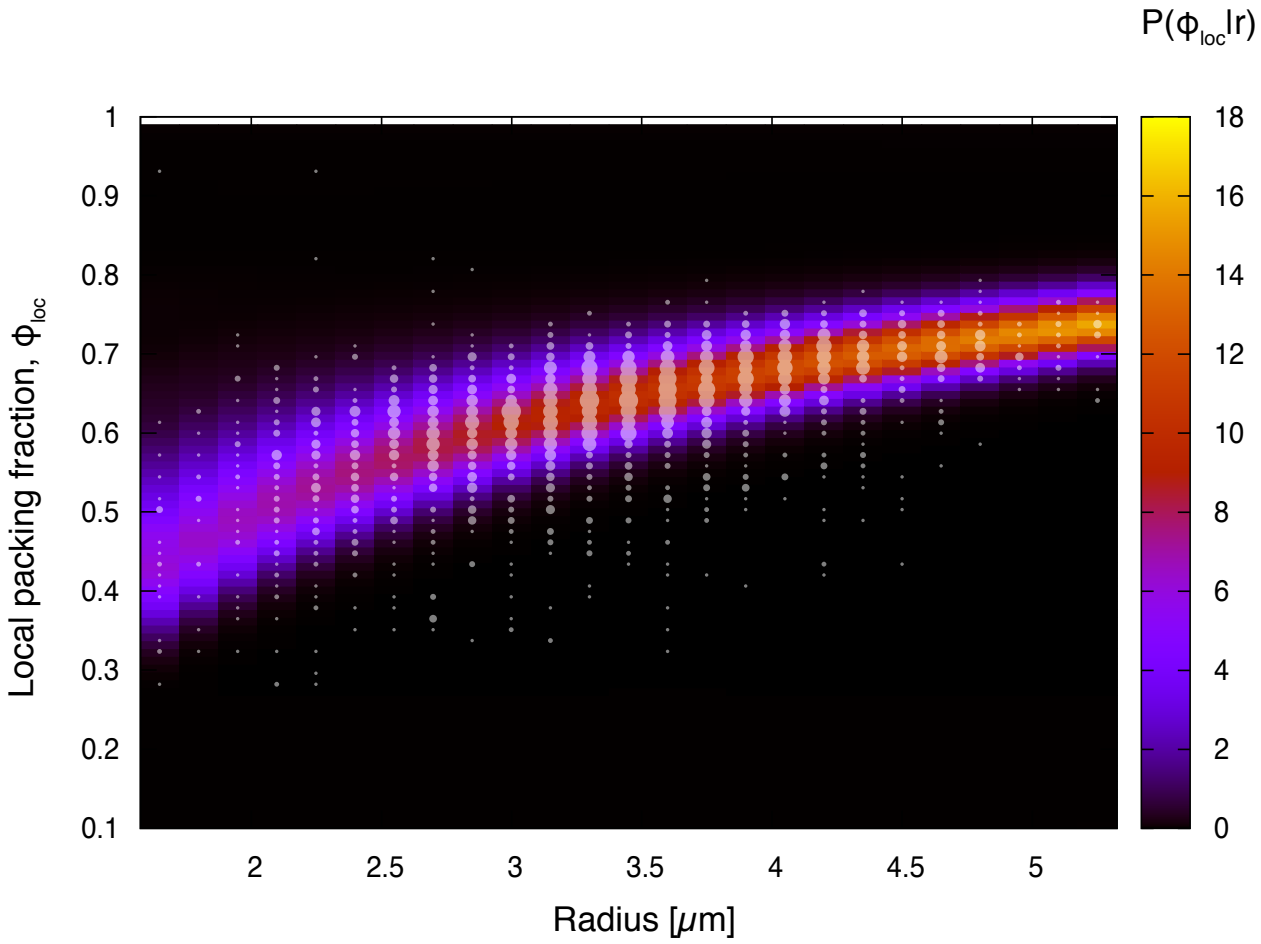

Figure A: **Local packing fraction distribution:** The colour map is the conditional probability density $P(\phi_{\rm loc}|r_{\rm c})$ obtained from the model using $\Omega_{\rm max} = 3.68\pi$ and $p = 0.41$, while the circles are the experimental points obtained for the emulsion presented in Figure 1. Their area is proportional to the number of observations.

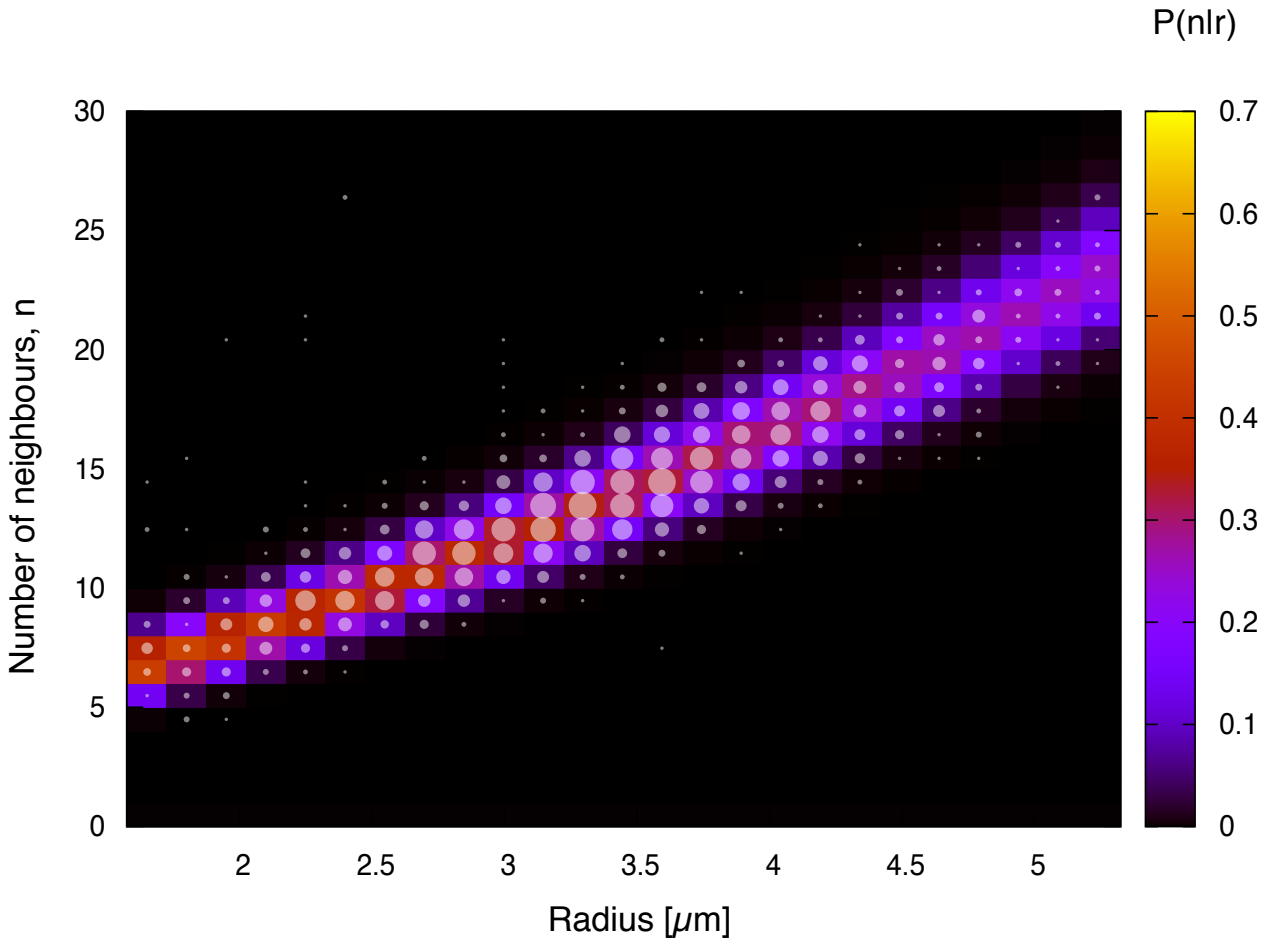

Figure B: **Number of neighbours distribution:** The colour map is the conditional probability density $P(n|r_c)$ obtained from the model using $\Omega_{max} = 3.68\pi$ and $p = 0.41$, while the circles are the experimental points obtained for the emulsion presented in Figure 1. Their area is proportional to the number of observations.

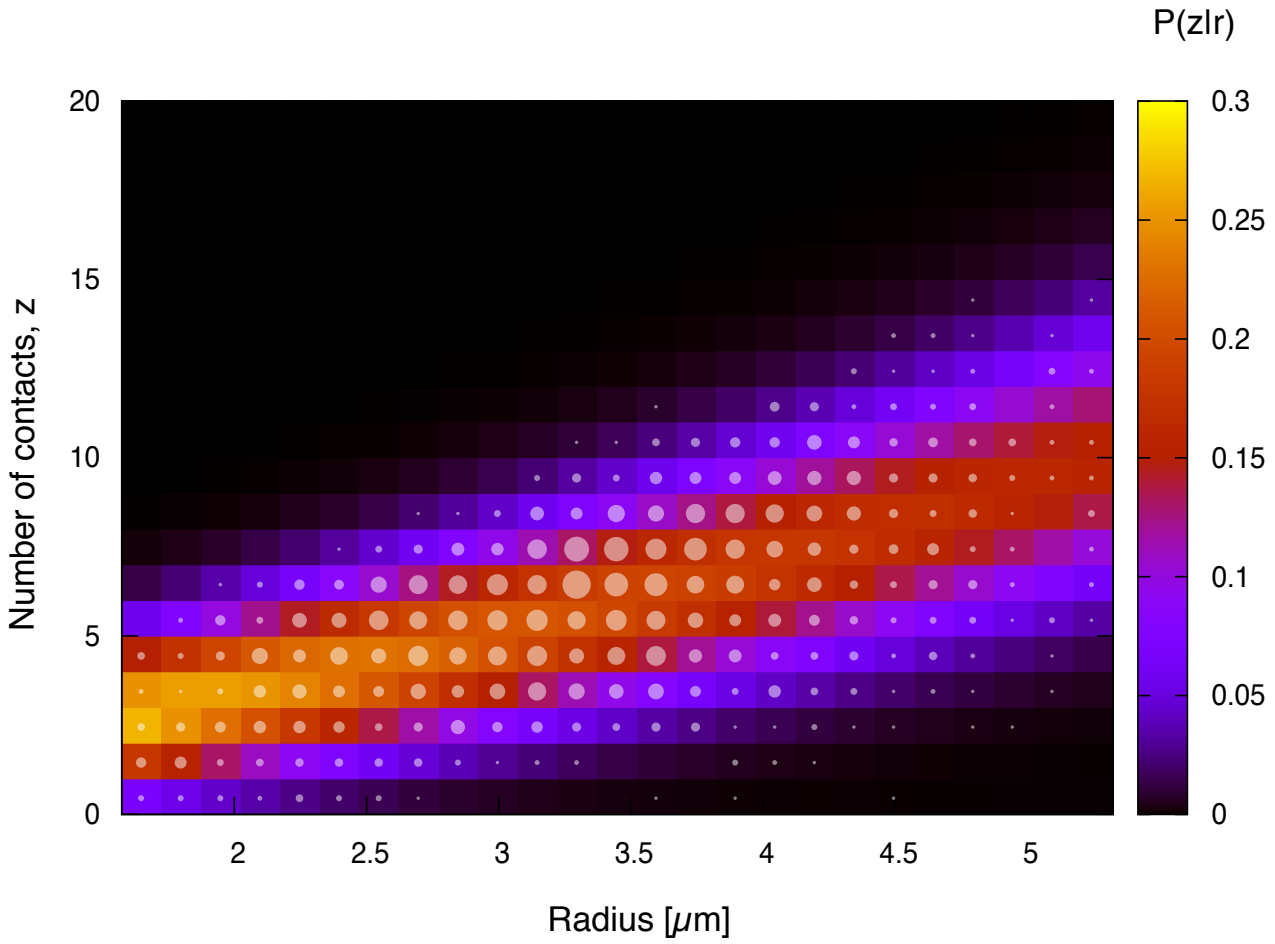

Figure C: **Number of contacts distribution:** The colour map is the conditional probability density $P(c|r_c)$ obtained from the model using $\Omega_{max} = 3.68\pi$ and $p = 0.41$, while the circles are the experimental points obtained for the emulsion presented in Figure 1. Their area is proportional to the number of observations.

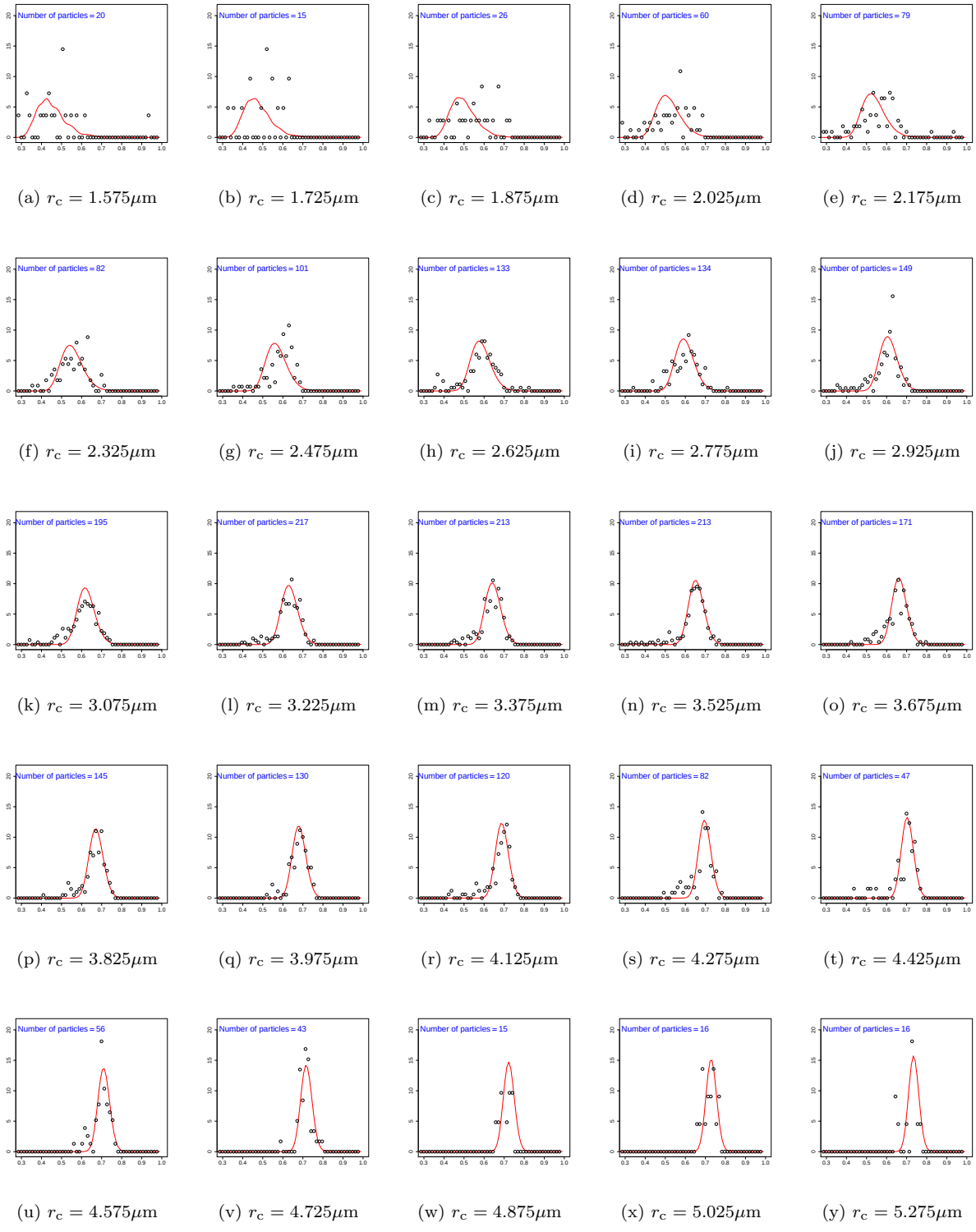

(a) $r_c = 1.575\mu$m (b) $r_c = 1.725\mu$m (c) $r_c = 1.875\mu$m (d) $r_c = 2.025\mu$m (e) $r_c = 2.175\mu$m

(f) $r_c = 2.325\mu$m (g) $r_c = 2.475\mu$m (h) $r_c = 2.625\mu$m (i) $r_c = 2.775\mu$m (j) $r_c = 2.925\mu$m

(k) $r_c = 3.075\mu$m (l) $r_c = 3.225\mu$m (m) $r_c = 3.375\mu$m (n) $r_c = 3.525\mu$m (o) $r_c = 3.675\mu$m

(p) $r_c = 3.825\mu$m (q) $r_c = 3.975\mu$m (r) $r_c = 4.125\mu$m (s) $r_c = 4.275\mu$m (t) $r_c = 4.425\mu$m

(u) $r_c = 4.575\mu$m (v) $r_c = 4.725\mu$m (w) $r_c = 4.875\mu$m (x) $r_c = 5.025\mu$m (y) $r_c = 5.275\mu$m

Figure D: **Local packing fraction**: Evolution of the local packing fraction distribution for a given r_c, $P(\phi|r_c)$, for different r_c. Plain line: model. Dots: experiments.

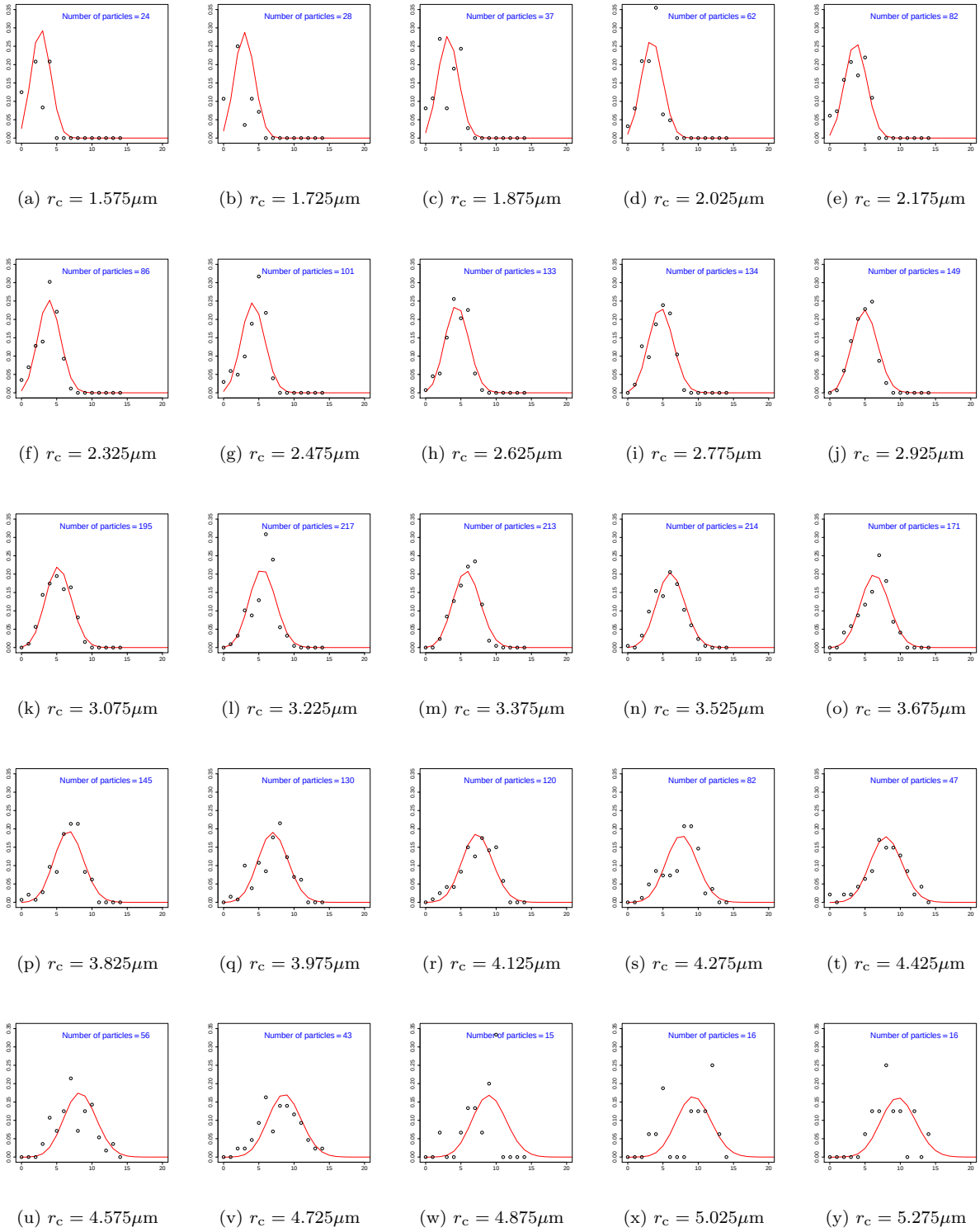

(a) $r_c = 1.575\mu m$ (b) $r_c = 1.725\mu m$ (c) $r_c = 1.875\mu m$ (d) $r_c = 2.025\mu m$ (e) $r_c = 2.175\mu m$

(f) $r_c = 2.325\mu m$ (g) $r_c = 2.475\mu m$ (h) $r_c = 2.625\mu m$ (i) $r_c = 2.775\mu m$ (j) $r_c = 2.925\mu m$

(k) $r_c = 3.075\mu m$ (l) $r_c = 3.225\mu m$ (m) $r_c = 3.375\mu m$ (n) $r_c = 3.525\mu m$ (o) $r_c = 3.675\mu m$

(p) $r_c = 3.825\mu m$ (q) $r_c = 3.975\mu m$ (r) $r_c = 4.125\mu m$ (s) $r_c = 4.275\mu m$ (t) $r_c = 4.425\mu m$

(u) $r_c = 4.575\mu m$ (v) $r_c = 4.725\mu m$ (w) $r_c = 4.875\mu m$ (x) $r_c = 5.025\mu m$ (y) $r_c = 5.275\mu m$

Figure E: **Contact number distribution**: Evolution of the contact number distribution for a given r_c, $P(z|r_c)$, for different r_c. Plain line: model. Dots: experiments.

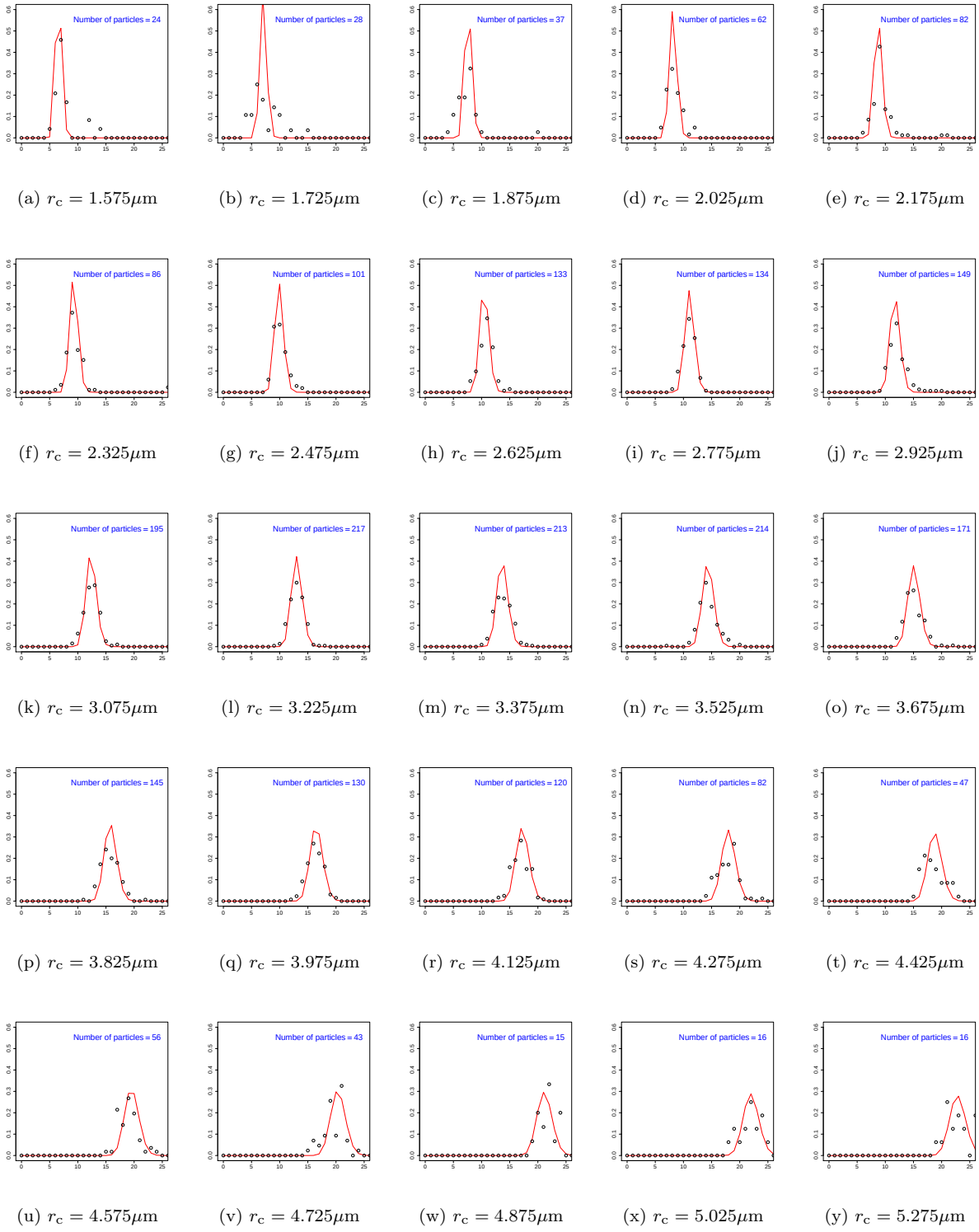

(a) $r_c = 1.575\mu m$ (b) $r_c = 1.725\mu m$ (c) $r_c = 1.875\mu m$ (d) $r_c = 2.025\mu m$ (e) $r_c = 2.175\mu m$

(f) $r_c = 2.325\mu m$ (g) $r_c = 2.475\mu m$ (h) $r_c = 2.625\mu m$ (i) $r_c = 2.775\mu m$ (j) $r_c = 2.925\mu m$

(k) $r_c = 3.075\mu m$ (l) $r_c = 3.225\mu m$ (m) $r_c = 3.375\mu m$ (n) $r_c = 3.525\mu m$ (o) $r_c = 3.675\mu m$

(p) $r_c = 3.825\mu m$ (q) $r_c = 3.975\mu m$ (r) $r_c = 4.125\mu m$ (s) $r_c = 4.275\mu m$ (t) $r_c = 4.425\mu m$

(u) $r_c = 4.575\mu m$ (v) $r_c = 4.725\mu m$ (w) $r_c = 4.875\mu m$ (x) $r_c = 5.025\mu m$ (y) $r_c = 5.275\mu m$

Figure F: **Neighbour number distribution**: Evolution of the Neighbour number distribution for a given r_c, $P(n|r_c)$, for different r_c. Plain line: model. Dots: experiments.

2 Other particle size distributions

The experimental samples we studied all present similar particle size distributions. In order to investigate the behaviour of our model for other distributions, we use numerical simulations to create jammed packings for controlled particle size distributions, using the LAMMPS molecular dynamics simulations [S. J. Plimpton, Fast Parallel Algorithms for Short-Range Molecular Dynamics, J Comp Phys, 117, 1-19 (1995), ¡http://lammps.sandia.gov/index.html¿]. These packings were analysed in the same way as experimental ones, and compared with the model calculations.

2.1 Log-normal distributions

Log-normal distributions offer a good statistical description of many polydisperse emulsions:

$$P(r) = \frac{1}{r\sigma\sqrt{2\pi}} \exp\left[-\frac{(\ln r - \mu)^2}{2\sigma^2}\right]. \quad (1)$$

For a fixed value of $\mu = 1$, we created four jammed packings for increasing values of σ, thus changing the polydispersity of the packing. Table 1 presents the value of $\langle \Omega_{\max} \rangle$ and $\langle p \rangle$ obtained for the different packings. These values clearly show that the set of parameters that characterize a packing weakly depends on the polydispersity. Note, however, that this variation is rather small, so that to a first approximation a reasonable description of the packing may be obtained by assuming the experimentally obtained values.

Figure G presents the comparison of the model and simulations for four different log-normal distributions with increasing variance. While the overall agreement is good, one can see that the model does not accurately predict the neighbour distribution when the sample is close to monodisperse. While the simulations exhibit a distribution of neighbours with a finite width, the model predicts a delta function. The proposed model is able to describe a polydisperse packing once the local source of randomness (poly-

σ	$\langle z \vert z \geq 4 \rangle$	$\langle \Omega_{\max} \rangle$	$\langle p \rangle$
0.01	6.5	3.74 π	0.468
0.1	6.5	3.65 π	0.463
0.2	6.6	3.52 π	0.470
0.3	6.5	3.34 π	0.454

Table 1: Values obtained for $\langle \Omega_{\max} \rangle$ and $\langle p \rangle$, for different values of σ.

dispersity) dominates the non-local one, coming from the long-range positional disorder. The neighbour distributions in all cases are fit to a high degree of accuracy, while the contact distributions show discrepancies when describing the mechanically unstable rattlers. This discrepancy may be a result of the protocol used to create the simulated packings, as we did not observe the same discrepancy in the experimental packings.

2.2 Gaussian distributions

Following Lochmann *et al.*, Solid State Sciences, **8** 1397 (2006), we performed numerical simulations for Gaussian distribution of sizes:

$$P(r) = \frac{1}{\sqrt{2\pi}\sigma} \exp\left(-\frac{(r-\mu)^2}{2\sigma^2}\right),$$

Such distributions are parameterized by $\eta = \sigma/\mu$. Results presented in Fig. H correspond to $\eta = 1, \quad 0.28$, to allow for a comparison with results by Lochmann *et al.*. Numerical simulations show excellent agreement with model predictions for both radii distributions and also capture the distributions presented in the literature.

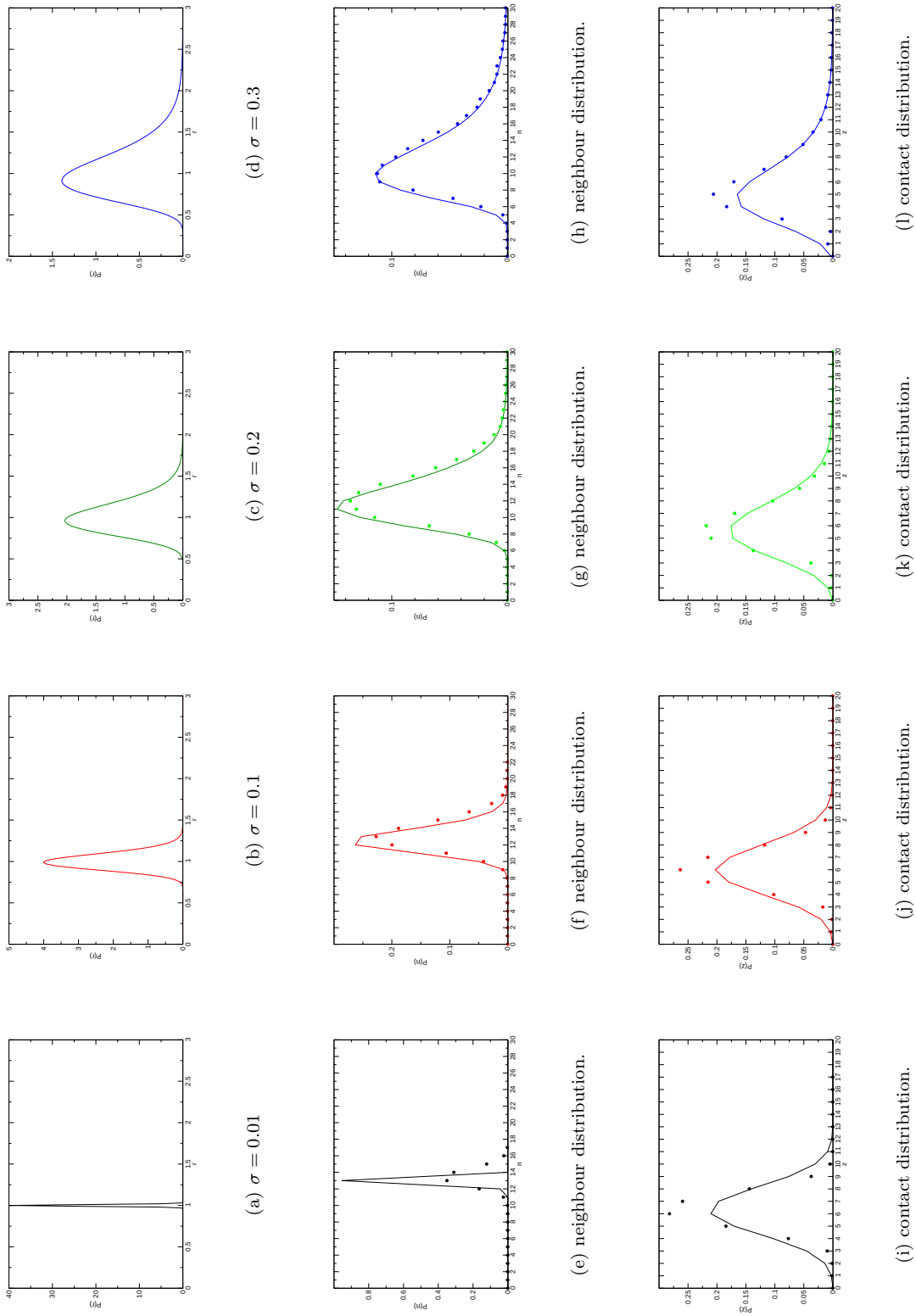

(a) $\sigma = 0.01$ (b) $\sigma = 0.1$ (c) $\sigma = 0.2$ (d) $\sigma = 0.3$

(e) neighbour distribution. (f) neighbour distribution. (g) neighbour distribution. (h) neighbour distribution.

(i) contact distribution. (j) contact distribution. (k) contact distribution. (l) contact distribution.

Figure G: **Log-normal distributions**: Comparison between model estimations (plain lines) and simulations (dots).

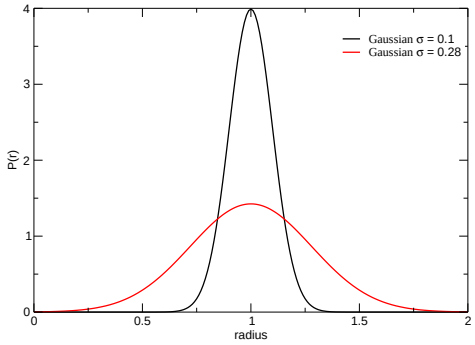

(a) Gaussian radius distributions

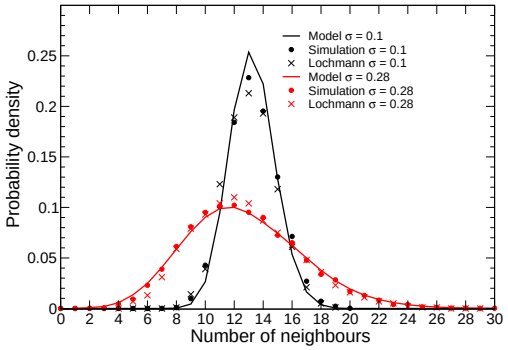

(b) Neighbour distributions.

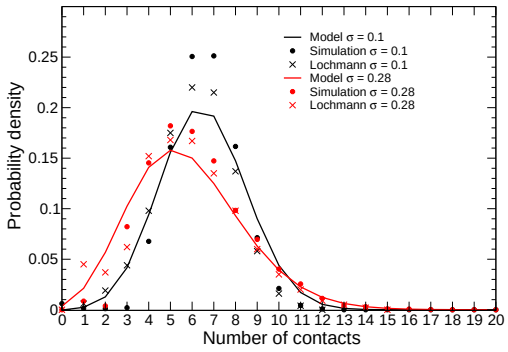

(c) Contact distributions.

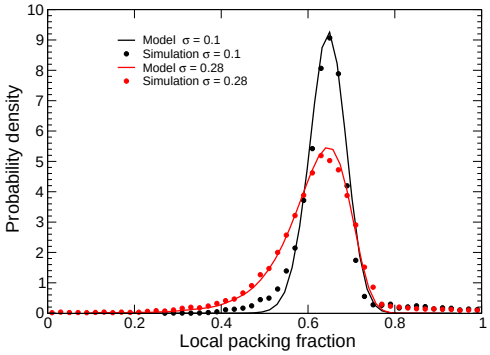

(d) Local packing fraction distributions.

Figure H: **Gaussian distributions**: Simulated radius distributions (a) and the corresponding probability densities for (b) the number of neighbours, (c) contacts, and (d) the local packing fraction. Model (plain line), numerical simulations (dots) and Lochmann *et al.* data (crosses).

2.3 Pareto distributions

Following Lochmann *et al.*, Solid State Sciences, **8** 1397 (2006), we performed numerical simulations for truncated power-law distributions, whose support is $[R_{\min}, R_{\max}]$:

$$P(r) = \begin{cases} \mathcal{N}(R_{\min}, R_{\max}, a) \quad r^{-a}, & \text{if } r \in [R_{\min}, R_{\max}] \\ 0, & \text{if } r \notin [R_{\min}, R_{\max}]. \end{cases}$$

It is parameterized by a and $\lambda = R_{\max}/R_{\min}$. Results presented on figure I corresponds to $a = 3.3$ and $\lambda = 5, \quad 9$, to allow for a comparison with results by Lochmann *et al.*. The model and the numerical simulations exhibit a good agreement.

3 Image analysis

The center point and radius of each droplet was measured from the confocal images using a deconvolution technique that is well suited to measurements on jammed systems. Each droplet was considered as the convolution of a delta-function at its center and a sphere of radius r. To make the measurements, we simply deconvolved the images to obtain the positions of all particles with a given radius r using the following procedure.

A test 3D volume was created with a sphere of radius r at its center. Gaussian noise was added to this test particle with similar characteristics to the noise found in the confocal image. Both volumes were transformed into the frequency domain where the Fourier transform of the confocal image was divided by the Fourier transform of the test volume. A tuned Weiner filter was applied to increase the signal relative to the noise. The resulting Fourier volume was then transformed back into the positional domain. In the resulting volume numerical approximations to delta-functions marked the center point of each droplet of radius r. This procedure was carried out for each radius r until every droplet in the volume was located.

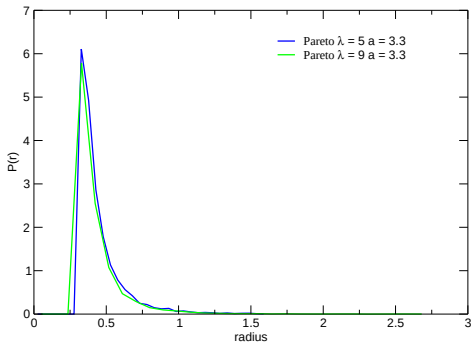

(a) Pareto radius distributions

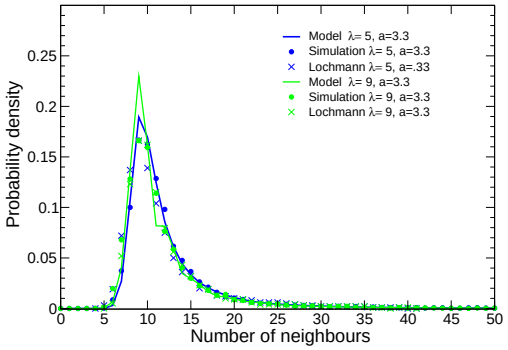

(b) Neighbour distributions.

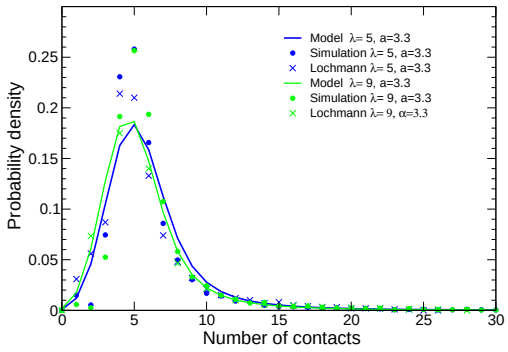

(c) Contact distributions.

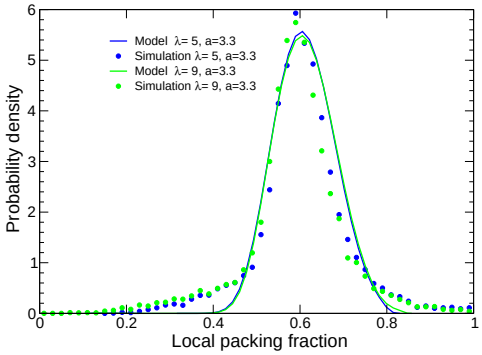

(d) Local packing fraction distributions.

Figure I: **Pareto distributions**: Simulated radius distributions (a) and the corresponding probability densities for (b) the number of neighbours, (c) contacts, and (d) the local packing fraction. Model (plain line), numerical simulations (dots) and Lochmann *et al.* data (crosses).

4 Recipe for application of the model

For practical purposes, such as optimizing the packing fraction by choosing the radius distribution (as is of interest to paint manufacturers), there exist a set of reasonable assumptions that yield realistic predictions. First, assume that both $\Omega_{\max}(r)$ and $p(r)$ are independent of r. Next, choose a value of $\Omega_{\max}$ slightly less than 4π to account for the presence of steric effects (e.g. 3.68π). Then it follows that $\langle n \rangle \simeq \Omega_{\max}/\langle \omega \rangle$, where $\langle \omega \rangle = \int dr\, dr_c\, \omega(r, r_c) P(r) P(r_c)$. Finally, assuming that a static packing is close to isostaticity, $\langle z \rangle \simeq 6$ and $p \simeq 6/\langle n \rangle$. In this way, the model can be exploited to make predictions about packings for a given distribution of particle sizes. This recipe will provide a good starting point for any experimental exploration. Using the bidisperse packings, we demonstrated that such an approximate method yielded good quantitative agreement with measured trends in the density dependence on the size ratio and the volume fraction of small particles.